Multilevel Monte Carlo convergence using high-order finite volume methods for elliptic PDEs with random coefficients

Prashant Kumar* Richard P. Dwight† Cornelis W. Oosterlee‡

Abstract

We present an approach to improve the convergence of a multilevel Monte Carlo method using a high-order discretization scheme for elliptic partial differential equations with random coefficients. We describe in detail a multilevel estimator which utilizes a fourth-order accurate solution of the elliptic PDEs. The superiority of this fourth-order estimator is reflected by fewer multilevel Monte Carlo levels and samples compared to the existing methods. Numerical experiments with small correlation length and high variance are reported.

Keywords: uncertainty quantification, high-order discretization, stochastic PDE, multilevel Monte Carlo

1 Introduction

Numerical simulation of a complex fluid flow process in a porous media is an important aspect of petroleum reservoir engineering and modeling of contaminant transport through aquifers. The outcome of these simulations becomes uncertain when the parameters involved in the mathematical models are not known deterministically. To deal with such uncertainty, we rely on sampling of these parameters based on some mean, variance and correlation structure and solving the model for each of those realizations. In order to get a reliable estimate of quantities, we need to consider a large number of samples as well as a very fine computational grid. This makes the problem computationally expensive. Recently, multilevel Monte Carlo (MLMC) methods have been developed to solve these types of problems efficiently [1, 2, 10]. Unlike direct methods, MLMC solves the problem on a hierarchy of grids such that most of the computations are done on relatively coarse grids and fewer on the finer grids.

The objective of this paper is to improve the convergence results for MLMC methods in [2] which employs a second-order accurate discretization to solve the elliptic PDE used to model the Darcy flow problem. We apply a fourth-order accurate finite volume (FV) scheme to the same problem. The advantage of using this high-order scheme is that the same accuracy can be achieved on a much coarser grid compared to low-order schemes resulting in fewer MLMC levels. Further, the MLMC estimator based on the fourth-order method shows convergence rates approximately twice that of the second-order estimator. Therefore, if an efficient solver for the fourth-order discretization is available, a large gain in computing time can be achieved over the existing method. This reasoning forms the main motivation for this work.

The layout of this paper is as follows. We begin by reviewing the subsurface flow problem and explain the quantity of interest in section 2. In section 3, we briefly explain the procedure to generate a Gaussian random field. In section 4, we describe in detail a second- and fourth-order accurate finite volume spatial discretization on a 2D Cartesian grid. Section 5 is devoted to the construction and analysis of MLMC estimators using the high-order finite volume scheme. In section 6, we provide some numerical experiments to test accuracy of our discretization and observe the convergence of multilevel methods for different test cases.

2 Problem setting

The mathematical model which determines the subsurface pressure distribution as a function of space is given by

$$-\nabla.(a\nabla u) = f, \qquad \text{in} \quad D \subset \mathbb{R}^d, \qquad d = 1, 2, 3, \tag{2.1}$$

*CWI – Centrum Wiskunde & Informatica, Amsterdam, the Netherlands, email: pkumar@cwi.nl,

†Faculty of Aerospace, Delft University of Technology, Delft, the Netherlands, e-mail: r.p.dwight@tudelft.nl,

‡CWI – Centrum Wiskunde & Informatica, Amsterdam, the Netherlands, email: c.w.oosterlee@cwi.nl, and Delft Institute of Applied Mathematics, Delft University of Technology.

where u is fluid pressure, a is the permeability (hydraulic conductivity), $a\nabla u$ together is called the Darcy velocity and f is the external rate of the flow. The boundary conditions are taken to be

$$u = g_D \qquad \text{in} \quad \Gamma^D \tag{2.2}$$

$$\frac{\partial u}{\partial \mathbf{n}} = g_N \qquad \text{in} \quad \Gamma^N \tag{2.3}$$

where Γ^D and Γ^N represent boundaries for Dirichlet and Neumann boundary conditions, respectively, and $\mathbf{n}$ denotes the outward normal to Γ^N. In the context of fluid flow problems, the Dirichlet boundary conditions represent the pressure values at inflow and outflow heads whereas the Neumann boundary conditions define the pressure gradient at the boundaries perpendicular to the main flow direction.

In order to numerically solve (2.1), we require the permeability at all locations in the computational domain. These permeability values are usually measured from borehole data at selected locations. Also, the heterogeneity in porous media restricts the extrapolation of these known values to nearby spatial locations. Therefore, a stochastic model is adapted to adequately represent these spatial variations. A realistic representation of a permeability field in any naturally occurring heterogeneous porous medium can be obtained by modeling it as a *log normal* random field [5]. This also ensures a positive permeability throughout the domain,

$$a(\mathbf{x}, \omega) = e^{Z(\mathbf{x},\omega)}, \qquad \mathbf{x} \in D, \tag{2.4}$$

where $Z(\mathbf{x}, \omega)$ is a *zero mean Gaussian random field* on D, ω is an event in the probability space $(\Omega, \mathcal{F}, \mathbb{P})$. For $Z(\mathbf{x}, \omega)$ we can define a covariance function $C : D \times D \to \mathbb{R}$ via:

$$C(\mathbf{x}, \mathbf{y}) = \mathrm{Cov}(Z(\mathbf{x}, \omega), Z(\mathbf{y}, \omega)) = \mathbb{E}[Z(\mathbf{x}, \omega)Z(\mathbf{y}, \omega)], \qquad \mathbf{x}, \mathbf{y} \in D. \tag{2.5}$$

In this paper, we will work with the Gaussian covariance functions:

$$C(\mathbf{x}, \mathbf{y}) = \sigma^2 e^{-\left(\frac{||\mathbf{x}-\mathbf{y}||}{\lambda}\right)^2}, \tag{2.6}$$

where parameters σ^2 and λ denote the *variance* and *correlation length*, respectively. The regularity of a random field is determined by the regularity of the covariance function. The Gaussian covariance function is C^∞ as a function of $||\mathbf{x} - \mathbf{y}||$ and results in a random field which is $C^\infty(\bar{D})$, $\bar{D} = [0, 1]^d$. We will discuss the techniques for sampling of random field in the next section.

The next task is to estimate statistics of certain functional $Q := \mathcal{X}(u)$ of the solution. In this paper, we consider as quantity of interest, Q, the expected value of outflow through the boundary Γ,

$$Q = \mathbb{E}\left[\int_\Gamma -a(\mathbf{x}, \omega)\nabla u(\mathbf{x}, \omega).\mathbf{n} \mathrm{d}S\right]. \tag{2.7}$$

The integral in above equation is also referred to as *effective permeability*. In physical terms, effective permeability is the permeability which gives the same flow through a homogeneous block as the flow through the heterogeneous block, D, when the boundary condition is constant pressure on inflow and outflow sides and no flow through the other sides of the block.

3 Sampling of the random field

In this section we describe a method for sampling of random field Z on a spatial grid. For a set of points $\{\mathbf{x}_i\}_{i=1}^M \in D$, where M is the total number of points on the grid, we define vector $\mathbf{Z} \in \mathbb{R}^M$ as

$$\mathbf{Z} = [Z(\mathbf{x}_1, \omega), Z(\mathbf{x}_2, \omega), ..., Z(\mathbf{x}_M, \omega)]^T, \tag{3.1}$$

and an $M \times M$ positive definite covariance matrix

$$\mathbf{C} = \mathbb{E}[\mathbf{Z}\mathbf{Z}^T] = \{C(\mathbf{x}_i, \mathbf{y}_j)\}_{i,j=1}^M. \tag{3.2}$$

We can factorize covariance matrix $\mathbf{C}$ to generate samples of $\mathbf{Z}$. This can be done by using a proper orthogonal decomposition :

$$\mathbf{C} = U\Lambda U^T, \tag{3.3}$$

where Λ is a diagonal matrix of ordered *eigenvalues* $\{\Lambda_{1,1} > \Lambda_{2,2} > ... > \Lambda_{M,M}\}$ and $U = [u_1, u_2, ..., u_M]$ is an $M \times M$ matrix whose columns u_i are *eigenvectors* of $\mathbf{C}$. The discrete Gaussian random field can now be formulated as

$$\mathbf{Z} = U\Lambda^{1/2}\xi, \qquad \xi \in \{\xi_1, ..., \xi_M\}, \qquad \xi_i \in \mathcal{N}(0, 1). \tag{3.4}$$

The above method gives an exact point-wise representation of the random field on an M point grid. The factorization is expensive, requires $\mathcal{O}(M^3)$ operations. Faster methods for factorization of $\mathbf{C}$ are also available which require only $\mathcal{O}(M \log M)$ operations, see [6, 12] for details.

4 Finite volume discretization

In subsurface flow modeling, finite volume methods are usually preferred over the finite element due to the local conservation property [4]. In this section we derive a finite volume approximation of the problem (2.1) using a second- and fourth-order discretization scheme in a 2D *cell-centered grid*.

We begin by dividing the domain D into control volumes or cells, that are squares of size h^2, with cell centers at points

$$D_h = \{(x, y) : x = x_i = (i - \tfrac{1}{2})h, y = y_j = (j - \tfrac{1}{2})h; i, j = 1, 2, ..., m; h = \tfrac{1}{m}\}. \tag{4.1}$$

The cell with center (x_i, y_j) is denoted as $D_{i,j}$ and its boundary as $\partial D_{i,j} = \bigcup_{\kappa=1}^{4} \partial D_{i,j,\kappa}$. In each of the finite volumes $D_{i,j}$, the integral formulation of (2.1) has the form

$$\int_{D_{i,j}} -\nabla.(a\nabla u)dD = \int_{D_{i,j}} f dD. \tag{4.2}$$

Using the Gauss divergence theorem, the left-hand side of the above integral is reformulated as a boundary integral for boundary $\partial D_{i,j,\kappa}$ and $\mathbf{n}_\kappa$ is the unit normal vector to that boundary

$$\int_{D_{i,j}} -\nabla.(a\nabla u)dD = -\sum_{\kappa=1}^{4} \int_{\partial D_{i,j,\kappa}} a\nabla u.\mathbf{n}_\kappa dS_\kappa. \tag{4.3}$$

For cell ABCD in Fig. 1, the boundary integrals are given by

$$-\sum_{\kappa=1}^{4} \int_{\partial D_{i,j,\kappa}} a\nabla u.\mathbf{n}_\kappa dS_\kappa = \int_A^B a\frac{\partial u}{\partial y}dx - \int_B^C a\frac{\partial u}{\partial x}dy - \int_C^D a\frac{\partial u}{\partial y}dx + \int_D^A a\frac{\partial u}{\partial x}dy. \tag{4.4}$$

We define the normal flux as $F^\kappa = a\nabla u.\mathbf{n}_\kappa$ and the so-called face-average normal flux as $\langle F^\kappa \rangle = \frac{1}{h}\int_{\partial D_{i,j,\kappa}} F^\kappa dS_\kappa$. Now, we can rewrite the integral form of the PDE in terms of face-averaged fluxes at face centers of cell ABCD,

$$h\left[\langle F^{AB}\rangle - \langle F^{BC}\rangle - \langle F^{CD}\rangle + \langle F^{DA}\rangle\right] = \int_{D_{i,j}} f dD. \tag{4.5}$$

The above relation is called *flux-balance* equation per volume which we discretize to second- and fourth-order accuracy in sections 4.1 and 4.2, respectively.

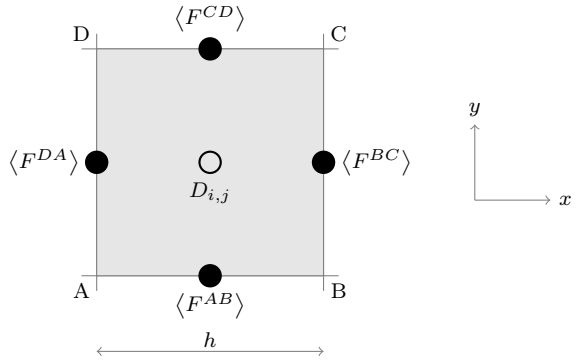

Fig. 1: A volume $D_{i,j}$ and face-averaged normal fluxes at face centers

4.1 Second-order discretization

To approximate (4.5) to second-order accuracy, we use a central difference scheme to compute the gradient $\nabla u.\mathbf{n}_\kappa$. For the face BC, we find

$$\langle F^{BC}\rangle^{(2)} = \frac{1}{h}\int_B^C a\frac{\partial u}{\partial x}dy \approx \frac{1}{h}\left[a_{i+\frac{1}{2},j}\left(\frac{u_{i+1,j} - u_{i,j}}{h}\right)h\right]. \tag{4.6}$$

Fluxes at other faces are approximated similarly. If the coefficient field is smooth, we can approximate $a_{i+\frac{1}{2},j}$ with the mean of $a_{i,j}$ and $a_{i+1,j}$. In case of discontinuous coefficients, a harmonic average $\bar{a}_{i+\frac{1}{2},j}$ of $a_{i,j}$ and $a_{i+1,j}$ works well [8]. The right-hand integral in (4.5) is approximated using a midpoint rule $\int_{D_{i,j}} f dD \approx h^2 f_{i,j}$. Finally, we get the discrete equation for volume $D_{i,j}$ as

$$-a_{i-\frac{1}{2},j}u_{i-1,j} - a_{i+\frac{1}{2},j}u_{i+1,j} + \Sigma_{i,j}u_{i,j} - a_{i,j-\frac{1}{2}}u_{i,j-1} - a_{i,j+\frac{1}{2}}u_{i,j+1} = h^2 f_{i,j}, \tag{4.7}$$

where $\Sigma_{i,j} = a_{i-\frac{1}{2},j} + a_{i+\frac{1}{2},j} + a_{i,j-\frac{1}{2}} + a_{i,j+\frac{1}{2}}$. For Dirichlet boundary conditions, i.e. $u = g_D$, we use a one-sided difference instead of central difference in Eq. (4.6). A Neumann boundary condition is applied by directly using g_N in place of the finite difference approximation.

4.2 Fourth-order discretization

We describe a fourth-order scheme for a regular 2D spatial grid. This approach can be extended to other more complex grid systems such as in mapped coordinates and locally-refined grids [3, 9]. To compute the face-averaged normal fluxes defined in Eq. (4.5), we use a fourth-order accurate quadrature rule. We will now explain in detail the computation of the face-averaged normal flux for the face BC:

$$\left\langle F^{BC} \right\rangle^{(4)} = F^{BC}_{i+\frac{1}{2},j} + \frac{h^2}{24} \left. \frac{\partial^2 F^{BC}}{\partial y^2} \right|_{i+\frac{1}{2},j} + \mathcal{O}(h^4), \tag{4.8}$$

where $\left. \frac{\partial^2 F^{BC}}{\partial y^2} \right|_{i+\frac{1}{2},j}$ is the transverse Laplacian of the flux at the center of face. We can write above formula as

$$\left\langle F^{BC} \right\rangle^{(4)} = a \left. \frac{\partial u}{\partial x} \right|_{i+\frac{1}{2},j} + \frac{h^2}{24} \left[\frac{\partial^2 a}{\partial y^2} \frac{\partial u}{\partial x} + 2 \frac{\partial a}{\partial y} \frac{\partial^2 u}{\partial y \partial x} + a \frac{\partial^3 u}{\partial y^2 \partial x} \right]_{i+\frac{1}{2},j} + \mathcal{O}(h^4). \tag{4.9}$$

Thus, the face-averaged flux is expressed in terms of a point-wise value of a and $\frac{\partial u}{\partial x}$ and their derivatives at the center of face. As the expansion in Eq. (4.8), one can also write

$$\langle a \rangle_{i+\frac{1}{2},j} = a_{i+\frac{1}{2},j} + \frac{h^2}{24} \left. \frac{\partial^2 a}{\partial y^2} \right|_{i+\frac{1}{2},j} + \mathcal{O}(h^4), \tag{4.10}$$

$$\left\langle \frac{\partial u}{\partial x} \right\rangle_{i+\frac{1}{2},j} = \left. \frac{\partial u}{\partial x} \right|_{i+\frac{1}{2},j} + \frac{h^2}{24} \left. \frac{\partial^3 u}{\partial y^2 \partial x} \right|_{i+\frac{1}{2},j} + \mathcal{O}(h^4). \tag{4.11}$$

Using (4.10) and (4.11), we can reduce (4.9) to

$$\left\langle F^{BC} \right\rangle^{(4)}_{i+\frac{1}{2},j} = \langle a \rangle_{i+\frac{1}{2},j} \left\langle \frac{\partial u}{\partial x} \right\rangle_{i+\frac{1}{2},j} + \frac{h^2}{12} \frac{\partial a}{\partial y} \left. \frac{\partial^2 u}{\partial y \partial x} \right|_{i+\frac{1}{2},j} + \mathcal{O}(h^4). \tag{4.12}$$

The above form has a smaller stencil size compared to Eq. (4.9).

4.2.1 Computation of $\langle \mathbf{a} \rangle_{\mathbf{i+\frac{1}{2},j}}$ and $\left. \frac{\partial \mathbf{a}}{\partial \mathbf{y}} \right|_{\mathbf{i+\frac{1}{2},j}}$

Assuming that the coefficient field is smooth and is sampled at cell-centered locations, we first interpolate the coefficient values at the face-centered location using a centered fourth-order finite difference, i.e.

$$a_{i+\frac{1}{2},j} = \frac{1}{16} \left[9(a_{i,j} + a_{i+1,j}) - (a_{i-1,j} + a_{i+2,j}) \right] + \mathcal{O}(h^4), \tag{4.13}$$

$$\left. \frac{\partial^2 a}{\partial y^2} \right|_{i+\frac{1}{2},j} = \frac{1}{h^2} \left[a_{i+\frac{1}{2},j-1} - 2a_{i+\frac{1}{2},j} + a_{i+\frac{1}{2},j+1} \right] + \mathcal{O}(h^2). \tag{4.14}$$

We can compute $\langle a \rangle_{i+\frac{1}{2},j}$ using (4.10). The term $\left. \frac{\partial a}{\partial y} \right|_{i+\frac{1}{2},j}$ only needs to be computed with $\mathcal{O}(h^2)$ accuracy. Therefore,

$$\left. \frac{\partial a}{\partial y} \right|_{i+\frac{1}{2},j} = \frac{1}{2h} [a_{i+\frac{1}{2},j+1} - a_{i+\frac{1}{2},j-1}] + \mathcal{O}(h^2). \tag{4.15}$$

4.2.2 Computation of $\left\langle \frac{\partial \mathbf{u}}{\partial \mathbf{x}} \right\rangle_{\mathbf{i+\frac{1}{2},j}}$

Using the same relation as Eq. (4.8), one can write

$$\left\langle \frac{\partial u}{\partial x} \right\rangle_{i+\frac{1}{2},j} = \left[\frac{\partial u}{\partial x} + \frac{h^2}{24} \frac{\partial^3 u}{\partial y^2 \partial x} \right]_{i+\frac{1}{2},j}. \tag{4.16}$$

Next, using the Tayler's expansion, we define

$$\rho_{i+\frac{1}{2},j} = \frac{1}{24}\left[27(u_{i+1,j} - u_{i,j}) - (u_{i+2,j} - u_{i-1,j})\right], \tag{4.17}$$

see Fig. 2 (*Left*) for the stencil. We can now use $\rho_{i+\frac{1}{2},j}$ for computing the elements in (4.16) as

$$\left.\frac{\partial u}{\partial x}\right|_{i+\frac{1}{2},j} = \frac{\rho_{i+\frac{1}{2},j}}{h} + \mathcal{O}(h^4), \tag{4.18}$$

$$\left.\frac{\partial^3 u}{\partial y^2 \partial x}\right|_{i+\frac{1}{2},j} = \frac{1}{h^3}\left[\rho_{i+\frac{1}{2},j-1} - 2\rho_{i+\frac{1}{2},j} + \rho_{i+\frac{1}{2},j+1}\right] + \mathcal{O}(h^2). \tag{4.19}$$

4.2.3 Computation of $\left.\frac{\partial^2 \mathbf{u}}{\partial \mathbf{y}\partial \mathbf{x}}\right|_{\mathbf{i+\frac{1}{2},j}}$

For this term, we use

$$\left.\frac{\partial^2 u}{\partial y \partial x}\right|_{i+\frac{1}{2},j} = \frac{1}{2h^2}\left[\rho_{i+\frac{1}{2},j+1} - \rho_{i+\frac{1}{2},j-1}\right] + \mathcal{O}(h^2). \tag{4.20}$$

This completes the fourth-order accurate face-averaged flux computation for face BC. Averaged fluxes at other faces are computed analogously. Finally, we obtain a 21-point stencil in a 5×5 block which is centered at the cell on which flux divergence is computed. In case of 1D problems, we do not have any transverse derivatives and we obtain a 5-point stencil. Regarding the right-hand side of the Eq. (4.5), we again use the fourth-order quadrature rule on the cell $D_{i,j}$, i.e.

$$\int_{D_{i,j}} f dD \approx h^2 \left[f + \frac{h^2}{24}\Delta f\right]_{i,j}, \tag{4.21}$$

where Δ is the Laplacian operator computed with a second-order accuracy.

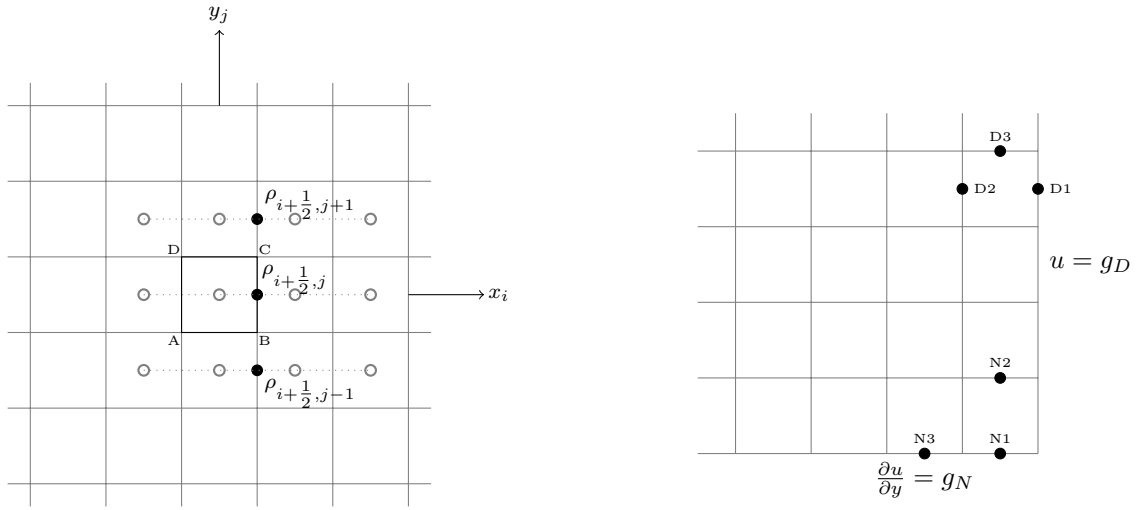

Fig. 2: *Left* Grid points at cell-centers required to compute $\langle \partial u/\partial x \rangle_{i+1/2,j}$ using (4.17). We get a 21-point stencil centered around cell ABCD. *Right* Points near or at the boundary which require stencil modification to incorporate boundary conditions.

4.2.4 Dirichlet boundary conditions

For Dirichlet boundary conditions, we use cubic polynomial interpolation. This results in a reduced accuracy at the boundaries while the overall order is still maintained due to elliptic regularity. Therefore, for the grid point labeled $D1$ in Fig. 2 (*Right*) we have

$$\rho_{m+\frac{1}{2},j} = \frac{1}{60}\left[184 g_{D_{m+\frac{1}{2},j}} - 225u_{m,j} + 50u_{m-1,j} - 9u_{m-2,j}\right]. \tag{4.22}$$

Using the same cubic interpolation for the point $D2$ in Fig. 2 (*Right*), we get

$$\rho_{m-\frac{1}{2},j} = \frac{1}{60}\left[-8 g_{D_{m+\frac{1}{2},j}} + 75u_{m,j} - 70u_{m-1,j} + 3u_{m-2,j}\right]. \tag{4.23}$$

Furthermore, for the point $D3$ in Fig. 2 (*Right*), we compute the transverse gradient term $\frac{\partial^2 u}{\partial x \partial y}\Big|_{m,j+\frac{1}{2}}$ using a one-sided second-order accurate formula, as follows,

$$\frac{\partial^2 u}{\partial x \partial y}\bigg|_{m,j+\frac{1}{2}} = \frac{1}{2h^2}\left[3\rho_{m,j+\frac{1}{2}} - 4\rho_{m-1,j+\frac{1}{2}} + \rho_{m-2,j+\frac{1}{2}}\right] + \mathcal{O}(h^2). \tag{4.24}$$

4.2.5 Neumann boundary conditions

In case of Neumann boundary conditions, we know the exact point-wise values of the flux at the face centers, i.e. $F = a\frac{\partial u}{\partial y}$. Therefore, we can use the formula in (4.8) directly. For the point labeled $N1$ in Fig. 2 (*Right*) the transverse Laplacian $\frac{\partial^2 F^{N1}}{\partial x^2}\Big|_{m,\frac{1}{2}}$ is computed with one-sided differences, whereas for point N3, $\frac{\partial^2 F^{N3}}{\partial x^2}\Big|_{m-1,\frac{1}{2}}$ is computed with the central difference operator. To construct the stencil for point N2, we first determine the value of $u_{m,\frac{1}{2}}$ using the stencil provided in (4.22) and $g_{N_{m,\frac{1}{2}}} = \frac{\partial u}{\partial y}\Big|_{m,\frac{1}{2}}$ as

$$\frac{\partial u}{\partial y}\bigg|_{m,\frac{1}{2}} = \frac{\rho_{m,\frac{1}{2}}}{h} = \frac{1}{60h}\left[184u_{m,\frac{1}{2}} - 225u_{m,1} + 50u_{m,2} - 9u_{m,3}\right]. \tag{4.25}$$

Now we can use $u_{m,\frac{1}{2}}$ in the stencil given in (4.23) to compute $\rho_{m,\frac{3}{2}}$. This completes the discretization in 2D.

5 Monte Carlo estimators

We will now briefly discuss the standard Monte Carlo (MC) and multilevel Monte Carlo (MLMC) methods. Readers are referred to [2, 7] for a more detailed derivation of these techniques.

Our computational goal is to compute the expected value of the outflow through the boundary as defined in (2.7) which depends on the solution of the Darcy flow equation. Thus, using the methods outlined in section 4, we approximate u on a mesh and compute $Q_h := \mathcal{X}(u_h)$. Further, we make an assumption that the discretization error in $\mathbb{E}[Q_h]$ decays *w.r.t* to mesh width as $\mathcal{O}(h^\alpha)$, i.e.

$$|\mathbb{E}[Q_h - Q]| = \mathcal{O}(h^\alpha), \qquad \alpha > 0, \tag{5.1}$$

where α can be obtained empirically by linear regression. We denote the decay rate obtained from second- and fourth-order schemes $\alpha^{(2)}$ and $\alpha^{(4)}$, respectively. For a smooth solution, we expect $\alpha^{(2)} < \alpha^{(4)}$, which we will confirm through our numerical results in the next section.

Table 1: Notation for (ML)MC-FV methods and respective mesh (hierarchy) width required to achieve a RMSE of ϵ

MC2	Monte Carlo method with second-order FV scheme	$h_L^{(2)} = \mathcal{O}(\epsilon^{1/\alpha^{(2)}})$
MC4	Monte Carlo method with fourth-order FV scheme	$h_L^{(4)} = \mathcal{O}(\epsilon^{1/\alpha^{(4)}})$
MLMC2	multilevel Monte Carlo method with second-order FV scheme	$h_\ell = h_L^{(2)} s^{(L-\ell)}$
MLMC4	multilevel Monte Carlo method with fourth-order FV scheme	$h_\ell = h_L^{(4)} s^{(L-\ell)}$

Next, we perform an error analysis for the Monte Carlo estimators and develop an algorithm combining the solutions from the FV schemes discussed in section 4 with the MC/MLMC method. Note that MC2 and MLMC2 given in Table 1 are the same estimators described in [2] and MC4 and MLMC4 are the estimators that we propose here.

5.1 Single level Monte Carlo method

We can define an unbiased Monte Carlo estimator, $\hat{Q}_{h,N}^{MC}$, of $\mathbb{E}[Q_h]$ which uses N realizations of the solution on a grid with mesh width h. Thus, the mean square error (MSE) of the MC estimator is given by

$$\mathcal{E}(\hat{Q}_{h,N}^{MC})^2 = \mathbb{E}[(\hat{Q}_{h,N}^{MC} - \mathbb{E}[Q_h])^2], \tag{5.2}$$

separating the error due to finite sampling and spatial discretization, the above expression can be expanded as

$$\mathcal{E}(\hat{Q}_{h,N}^{MC})^2 = \mathbb{V}[\hat{Q}_{h,N}^{MC}] + (\mathbb{E}[Q_h - Q])^2 = \frac{\mathbb{V}[Q_h]}{N} + (\mathbb{E}[Q_h - Q])^2, \tag{5.3}$$

where $\mathbb{V}[Q_h]$ is the sample variance. In order to achieve an MSE of $\mathcal{E}(\hat{Q}_{h,N}^{MC})^2 < \epsilon^2$, we need to choose a grid $h = \mathcal{O}(\epsilon^{1/\alpha})$ and a number of samples $N = \mathcal{O}(\epsilon^{-2})$ assuming $\mathbb{V}[Q_h]$ is constant, independent of the grid size. We also note that the fourth-order scheme will converge to ϵ on a coarser grid due to larger α, i.e. $h^{(4)} > h^{(2)}$.

Since the cost to compute one sample of Q_h grows as $\mathcal{O}(h^{-\gamma})$, $\gamma \geq 1$, the computational cost to achieve an accuracy of ϵ by MC method is given by

$$\mathcal{C}_\epsilon^{MC} = \mathcal{O}(Nh^{-\gamma}) = \mathcal{O}(\epsilon^{-2-\gamma/\alpha}). \tag{5.4}$$

Putting these insights together we now provide the MC2/MC4 algorithms that consist of the following three steps:

1. **Sampling:** We generate N independent samples of permeability field $a(\cdot, \omega^{(i)})$, $\omega^{(i)} \in \Omega$, $i \in \{1, 2, ..., N\}$, on a suitable spatial grid $h_L^{(\nu)} := h^{(\nu)}$ from the FV discretization order $\nu = \{2, 4\}$.
2. **Finite Volume Solution:** For each realization of $a(\cdot, \omega^{(i)})$, the PDE in (2.1) is solved numerically by the solver of order ν. Then, we compute the quantity of interest (e.g. the effective outflow through the boundary) and denote the samples obtained by $Q^i_{h^{(\nu)}}$.
3. **Estimate Statistics:** We estimate the expectation of Q by the sample mean

$$\hat{Q}^{MC}_{h^{(\nu)},N} = \mathbb{E}_N[Q_{h^{(\nu)}}] = \frac{1}{N}\sum_{i=1}^{N} Q^i_{h^{(\nu)}}. \tag{5.5}$$

It is important to note that the computational cost of the standard MC method scales with the mesh width and sample size. So, a higher value of α can give the same accuracy on a coarser grid and can make the MC simulation significantly cheaper. For example, in a deterministic setting, a discretization accuracy of $\mathcal{O}(h^2)$ on an 256×256 grid is essentially the same as that of the $\mathcal{O}(h^4)$ discretization on 16×16 grid. But solving the 16×16 problem with fourth-order accuracy is typically cheaper than solving the 256×256 problem with second-order discretization. The fourth-order scheme may still be cheaper if its solver is slightly sub-optimal compared to the second-order solver, i.e. $\gamma^{(4)} > \gamma^{(2)}$ [11]. For all our computations, we use the sparse direct solver available with MATLAB to solve the linear system obtained from second- and fourth-order discretization. This solver is optimal for 1D problems with $\gamma^{(2)} \approx \gamma^{(4)} \approx 1$. Multigrid solution are part of a forthcoming paper.

5.2 Multilevel Monte Carlo method

While single level MC methods are easy to implement they tend to "over-resolve" the problem. The improved efficiency of the MLMC method comes from building the estimate of Q on a hierarchy of grids or levels, in a way which minimizes the overall variance for a given computational cost. It exploits the linearity of the expectation operator, i.e.

$$\mathbb{E}[Q_L] = \mathbb{E}[Q_{h_0}] + \sum_{\ell=1}^{L} \mathbb{E}[Q_{h_\ell} - Q_{h_{\ell-1}}], \tag{5.6}$$

where $h_\ell = s^{-1}h_{\ell-1}$, $s \in \mathbb{N}/\{1\}$ and $\ell \in \{0, 1, ..., L\}$. Each of the expectations in the above expression is independently computed with varying sample size N_ℓ. For small values of ℓ, expectations are inexpensive to compute accurately, because the PDE is solved on a very coarse grid. In turn, for large values of ℓ, where the numerical solution is expensive, only a few realizations are required assuming the variance of the correction term converges as $\mathbb{V}[Q_{h_\ell} - Q_{h_{\ell-1}}] = \mathcal{O}[h^\beta]$ with $\beta > 0$. As the expectations are independently computed, the MSE for the multilevel estimator can be quantified as

$$\mathcal{E}(\hat{Q}_L^{ML})^2 = \left(\frac{\mathbb{V}[Q_{h_0}]}{N_0} + \sum_{\ell=1}^{L} \frac{\mathbb{V}[Q_{h_\ell} - Q_{h_{\ell-1}}]}{N_\ell}\right) + (\mathbb{E}[Q_h - Q])^2. \tag{5.7}$$

From the above expression it can be observed that the finest grid required in the case of the MLMC method is the same as for the standard MC method. Further, as $h^{(4)} > h^{(2)}$, we get a smaller overall number of levels, L, for the fourth-order scheme keeping grid the multiplicity factor s from Eq. (5.9) same for both methods.
The computational cost to achieve an accuracy ϵ using an MLMC estimator is then given by

$$\mathcal{C}_\epsilon^{ML} = \mathcal{O}\left(N_0 h_0^{-\gamma} + \sum_{\ell=1}^{L}(N_\ell h_\ell^{-\gamma} + N_{\ell-1}h_{\ell-1}^{-\gamma})\right). \tag{5.8}$$

Proofs for the asymptotic computational cost of the MLMC method can be found in the appendix of [2]. Next, we provide the multilevel estimator for Q. The MLMC2/MLMC4 algorithms consist of following four steps:

1. **Mesh Hierarchy:** We consider a hierarchy of grids on D with mesh widths $h_\ell^{(\nu)}$ that satisfy

$$h_\ell^{(\nu)} = s^{-1} h_{\ell-1}^{(\nu)}. \tag{5.9}$$

2. **Sampling:** For each level of resolution ℓ, we generate N_ℓ independent samples of $a(\cdot, \omega^{(i)})$ with $i \in \{1, 2, ..., N_\ell\}$ on the grid with mesh width $h_\ell^{(\nu)}$.

3. **Finite Volume Solution:** For each mesh $h_\ell^{(\nu)}$ and realization $a(\cdot, \omega^{(i)})$, the elliptic PDE is solved numerically by solvers of order ν. We denote the ith sample of the quantity of interest as $Q^i_{h_\ell^{(\nu)}}$. We also generate the coarse grid version of $a(\cdot, \omega^{(i)})$ using the same random sample $\omega^{(i)} \in \Omega$ on level $\ell - 1$ ($\ell > 0$) and compute the coarse grid version $Q^i_{h_{\ell-1}^{(\nu)}}$.

4. **Estimate Statistics:** We estimate the expectation of Q using the following multilevel estimator:

$$\hat{Q}^{ML}_{L^{(\nu)}} = \mathbb{E}^L[Q_{h^{(\nu)}}] = \mathbb{E}_{N_0}[Q_{h_0^{(\nu)}}] + \sum_{\ell=1}^{L} \mathbb{E}_{N_\ell}[Q_{h_\ell^{(\nu)}} - Q_{h_{\ell-1}^{(\nu)}}] \tag{5.10}$$

with $\mathbb{E}_{N_\ell}$ being the MC estimator defined in (5.5) for level ℓ.

Remarks: In the present implementation, we numerically solve the problem in two consecutive mesh levels by adopting a suitable coarsening scheme for the random permeability field. For the 1D case, the coarsening of the permeability field can be done by injection on the cell faces. Another efficient way of doing this is by using an optimal multigrid solver such as Full Multigrid (FMG) with the same mesh hierarchy and utilizing the solution on the last two finest grids.

6 Numerical results

In this section we provide some numerical results to analyze the effectiveness of the methods described in the preceding sections. For all our results, we consider problem (2.1) on $D = (0, 1)$ with $f = 0$ and boundary conditions $u(0) = 1$ and $u(1) = 0$. We model permeability a as a continuous log normal field, such that $\log a$ has a Gaussian covariance function (2.6).

We first start by testing the accuracy of our discretization method. We consider different choices of correlation lengths $\lambda \in \{1/32, 1/64, 1/128\}$ to study the impact of a decreasing spatial regularity on the solution error. To compute the solution error we proceed in the following way. First we generate the permeability field on a relatively fine grid $h^* = 1/2048$, solve the PDE on that grid and use it as the reference. Next we solve the corresponding PDE with the coarse grid version of the permeability field on grids $h = \{1/16, 1/32, ..., 1/1024\}$ and evaluate the solution error with respect to the solution obtained on grid h^*. Fig. 3. shows the convergence results of the second- and fourth-order schemes in 1D. The expected value of the solution error increases with

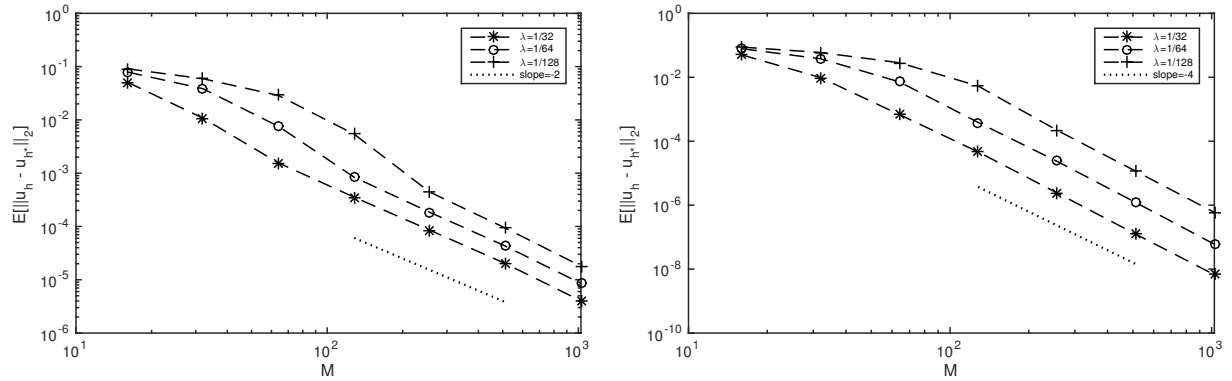

Fig. 3: Convergence of $\mathbb{E}[||u_h - u_{h^*}||_2]$, $h^* = 1/2048$ for second-order discretization (*Left*) and fourth-order discretization (*Right*) with different choices of correlation lengths λ and for $\sigma^2 = 1$.

decrease in the correlation lengths but the order of convergence is still preserved. For the case where $h > \lambda$, the convergence order is slightly affected as coarser grids are unable to resolve the low correlation lengths.

Now we examine in detail the performance of the MLMC-FV methods to compute the expected value of the quantity of interest, $Q = a\frac{du}{dx}\big|_{x=1}$ from Eq. (2.7) . Fig. 4 shows the result for the case with $\sigma^2 = 1$, $\lambda = 0.2$ and coarsest grid $h_0 = 1/8$. The left-side plot shows the behavior of $\mathbb{E}[Q_{h_\ell} - Q_{h_{\ell-1}}]$ for MLMC2 and MLMC4.

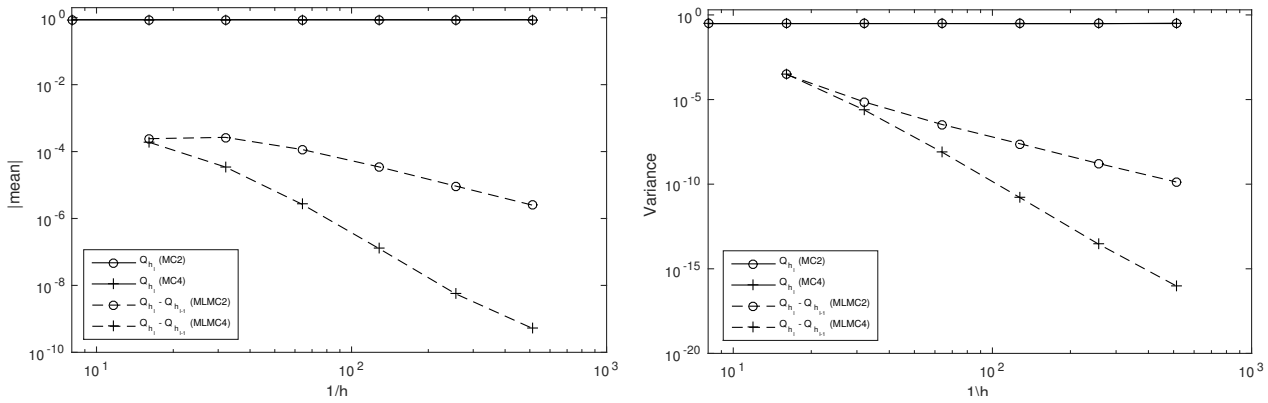

Fig. 4: Convergence rates for MLMC2 and MLMC4 methods with log normal permeability field generated using Gaussian covariance function with $\sigma^2 = 1$, $\lambda = 0.2$ and coarsest grid $h_0 = 1/8$. The quantity of interest is $Q = -a(du/dx)_{x=1}$. *Left* For $\mathbb{E}[Q_{h_\ell} - Q_{h_{\ell-1}}]$ the parameter $\alpha^{(2)} = 1.93$ and $\alpha^{(4)} = 4.22$. *Right* For $\mathbb{V}[Q_{h_\ell} - Q_{h_{\ell-1}}]$ the parameter $\beta^{(2)} = 3.87$ and $\beta^{(4)} = 8.65$.

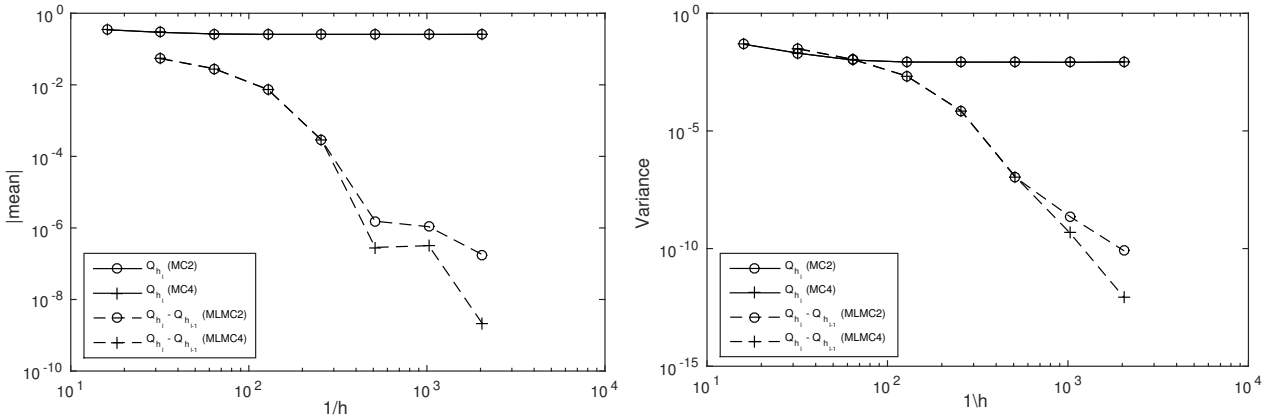

Fig. 5: Plots for $\mathbb{E}[Q_{h_\ell}]$ and $\mathbb{E}[Q_{h_\ell} - Q_{h_{\ell-1}}]$ (*Left*) as well as $\mathbb{V}[Q_{h_\ell}]$ and $\mathbb{V}[Q_{h_\ell} - Q_{h_{\ell-1}}]$ (*Right*) for the same test problem in 4 with $\lambda = 0.01$, $\sigma^2 = 3$ and coarsest grid $h_0 = 1/16$.

The slope of the line obtained from the MLMC2 method is -1.93, or $\alpha^{(2)} \approx 1.93$ and for MLMC4 is -4.22, or $\alpha^{(4)} \approx 4.22$. We also observe that $\mathbb{E}[Q_{h_\ell}]$ is approximately constant for the MC2 and MC4 methods. In the right-side plot we observe the convergence of $\mathbb{V}[Q_{h_\ell} - Q_{h_{\ell-1}}]$ for MLMC2 with slope -3.87, or $\beta^{(2)} \approx 3.87$ and for MLMC4 with slope -8.65, or $\beta^{(4)} \approx 8.65$. Also the $\mathbb{V}[Q_{h_\ell}]$ is approximately constant for the MC2 and MC4 methods.

Plots in Fig. 5 show the convergence rates for a relatively more difficult test case. We use a small correlation length $\lambda = 0.01$ and a higher variance $\sigma^2 = 3$ with coarsest grid $h_0 = 1/16$. For both methods, MLMC2 and MLMC4, we observe that $\mathbb{V}[Q_{h_\ell} - Q_{h_{\ell-1}}] > \mathbb{V}[Q_{h_\ell}]$ for coarser grids $h > \lambda$. In this case multilevel methods will be more expensive compared to the standard methods. To benefit from multilevel methods the coarsest grid should be chosen as $h_0 \approx \lambda$. We also observe that on coarser grids both methods, MLMC2 and MLMC4, exhibit similar convergence but MLMC4 outperforms MLMC2 when the problem is well resolved.

Now we compare the computational cost required to achieve the same accuracy ϵ for the MLMC2 and MLMC4 methods. Fig. 6 shows the number of MLMC levels and samples required to achieve different accuracy levels. The left-side plot shows results for the easy test case ($\lambda = 0.2$ and $\sigma^2 = 1$) from Fig. 4. We can see that the number of samples on the coarsest grid $h_0 = 1/8$ is almost the same, as $\mathbb{V}[Q_{h_0}](\text{MC2}) \approx \mathbb{V}[Q_{h_0}](\text{MC4})$. Further, we observe that the number of samples for MLMC4 decays more rapidly with the increasing grid size and converges to ϵ on a much coarser grid compared to MLMC2. The cost to compute one sample for both methods grows at the same rate in 1D, i.e. $\gamma^{(2)} \approx \gamma^{(4)}$ thus, making the fourth-order scheme more efficient. The right-side plot shows the result for the harder test case ($\lambda = 0.01$ and $\sigma^2 = 3$) from Fig. 5. We start with $h_0 = 1/64$ in order to see some benefit from the MLMC method. The gain from the MLMC4 method only becomes evident from finer grids onward. Both plots follow a similar trend as their respective variance plots.

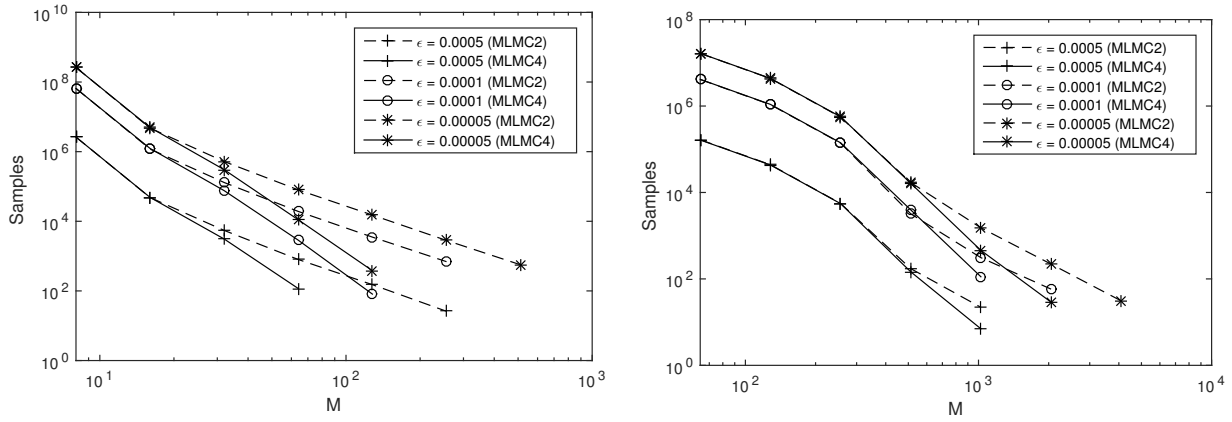

Fig. 6: Plot showing the number of samples and grid levels required to achieve a RMSE of ϵ using MLMC2 and MLMC4 methods. *Left* plot shows the result for the case in Fig. 4 with $h_0 = 1/8$. *Right* plot shows the result for the case in Fig. 5 with $h_0 = 1/64$.

7 Conclusion

We have outlined a strategy for the construction of fourth-order MLMC-FV methods for uncertainty quantification of subsurface flow problems. Our results indicate that the MLMC convergence rates for smooth coefficient fields can be improved by a factor of 2 using these high-order schemes. Even for standard Monte Carlo methods, the size of computational grids can be reduced significantly by using a fourth-order method instead of the second-order discretization. Our numerical results suggest that the high-order method also performs very well for small correlation lengths and high variance scenarios.

References

[1] A. Barth, C. Schwab, and N. Zollinger, *Multilevel Monte Carlo finite element method for elliptic PDE's with stochastic coefficients*, Numer. Math., 119 (2011), pp. 123–161.

[2] K. Cliffe, M. Giles, R. Scheichl, and A. Teckentrup, *Multilevel Monte Carlo methods and applications to elliptic PDEs with random coefficients*, Comput. Vis. Sci., 14 (2011), pp. 3–15.

[3] P. Colella, M. Dorr, J. Hittinger, and D. Martin, *High-Order, Finite-Volume Methods in Mapped Coordinates*, J. Comput. Phys., 230 (2011), pp. 2952–2976.

[4] G. Dagan, *Flow and Transport in Porous Formations*, Springer, (1989).

[5] P. Delhomme, *Spatial variability and uncertainty in groundwater flow parameters, a geostatistical approach*, Water Resourc. Res., (1979), pp. 269–280.

[6] C. Dietrich and G. Newsam, *Fast and exact simulation of stationary Gaussian processes through circulant embedding of the covariance matrix*, Siam J. Sci. Comput., 18 (1997), pp. 1088–1107.

[7] M. Giles, *Multilevel Monte Carlo path simulation*, Operations Research, 256 (2008), pp. 981–986.

[8] M. Khalil and P. Wesseling, *Vertex-Centered and Cell-Centered Multigrid for Interface Problems.*, J. Comput. Phys., 98 (1992), pp. 1–10.

[9] P. McCorquodale and P. Colella, *A high-order finite-volume method for hyperbolic conservation laws on locally-refined grids*, Comm. Appl. Math. Comput. Sci., Vol. 6, No. 1 (2011), pp. 1–25.

[10] A. Teckentrup, R. Scheichl, M. Giles, and E. Ullmann, *Further analysis of multilevel Monte Carlo methods for elliptic PDEs with random coefficients*, Numerische Mathematik, 125 (2013), pp. 569–600.

[11] U. Trottenberg, C. Oosterlee, and A. Schuller, *Multigrid*, Elsevier Academic Press, San Diego, CA, 2000.

[12] A. Wood and G. Chan, *Simulation of stationary Gaussian processes in* $[0,1]^d$, Journal of Computational and Graphical Statistics, 3 (1994), pp. 409–432.